DYNAMICS TOPOGRAPHY MONITORING IN PEATLAND USING THE LATEST DIGITAL TERRAIN MODEL

Atriyon Julzarika
Department of Geodetic Engineering, Universitas Gadjah Mada (UGM), Yogyakarta, Indonesia
National Research and Innovation Agency (BRIN), Cibinong, Indonesia

Harintaka Harintaka
Department of Geodetic Engineering, Universitas Gadjah Mada (UGM), Yogyakarta, Indonesia

Trias Aditya
Department of Geodetic Engineering, Universitas Gadjah Mada (UGM), Yogyakarta, Indonesia

Subaryono Subaryono
Department of Geodetic Engineering, Universitas Gadjah Mada (UGM), Yogyakarta, Indonesia

Cite article:

Julzarika A., Aditya T., Subaryono S., Harintaka H. (2022) DYNAMICS TOPOGRAPHY MONITORING IN PEATLAND USING THE LATEST DIGITAL TERRAIN MODEL, *Journal of Applied Engineering Science*, 20(1), 246 - 253, DOI:10.5937/ jaes0-31522

Online aceess of full paper is available at: *www.engineeringscience.rs/browse-issues*

DYNAMICS TOPOGRAPHY MONITORING IN PEATLAND USING THE LATEST DIGITAL TERRAIN MODEL

Atriyon Julzarika[1,2]*, Trias Aditya[1], Subaryono Subaryono1, Harintaka Harintaka[1]
[1]Department of Geodetic Engineering, Universitas Gadjah Mada (UGM), Yogyakarta, Indonesia
[2]National Research and Innovation Agency (BRIN), Cibinong, Indonesia

The Central Kalimantan province in Indonesia has one of the country's largest peatlands. The Peatland has dynamic topographic conditions that cause land subsidence or uplift in water levels. Monitoring the topographic dynamics conditions of this Peatland requires an up-to-date DTM capable of presenting the latest conditions. Monitoring with the latest DTM is needed because there is currently no method suited to large-scale, cost-effective mapping. This study aims to monitor the dynamics of topography in Peatland using the latest DTM. The latest DTM is a combination of the DTM master and the latest displacement. The novelty of this research is in monitoring the dynamics of Peatland with the latest DTM every rainy and dry season. DTM master is DTM extracted from InSAR ALOS PALSAR-2. Displacement was obtained from DInSAR extraction from Sentinel-1. The research area is located in Pulang Pisau, Indonesia. DTM master was extracted using InSAR in December 2017. Displacement was extracted every 6–7 months. The monitoring periods for dynamics topographic were January 2018, August 2018, January 2019, July 2019, January 2019, and June 2020. Each period involved extracting the latest DTM and the displacement. The dynamics topography of the study area lies at the value of 1.5 m. This latest DTM can be used for 1: 20,000 to 1: 25,000 mapping. The latest DTM has a RMSE(z) of 0.705 m on the field measurement. This vertical accuracy-test uses 15 points from GNSS-levelling. Based on the RMSE (z) obtained, the vertical accuracy is 1.3818 m at the 95% confidence level.

Key words: dynamic topography, the latest DTM, Peatland, Pulang Pisau, land subsidence

INTRODUCTION

The Peatland is a landscape composed of the imperfect decomposition of vegetation from waterlogged trees so that the conditions are anaerobic [1], [2]. The organic material continues to accumulate for a long time to form layers with a thickness of more than 50 cm [3], [4]. Peatlands are a type of wetlands, which are among the most valuable ecosystems on Earth, and are generally located between two major rivers [5]. They are critical for preserving global biodiversity, providing safe drinking water, minimizing flood risk, and addressing climate change as the largest natural terrestrial carbon store [2]. Peatlands in Indonesia are found in the lowlands and highlands. In general, lowland peat swamps are found in tidal swamps and humidifying swamps, located between two large rivers in the physiography or landform of the back of the river (back swamp), swamp behind the beach (swalle), humidification plains (closed basin), and coastal plain [6]. Currently, Peatland presents one of the main ecological problems in Indonesia. Various incidents such as land fires, mining, floods, land subsidence, and water quality have occurred on Indonesia's Peatland [7], [8]. One of Indonesia's most extensive peatlands is located in Pulang Pisau Regency, which has the largest peat dome and a depth of > 25 m [9]. Pulang Pisau is located in Central Kalimantan Province, see Figure 1. This district has an area of 8,997 km² [9]. The geological map of the area shows that the geological formations in Pulang Pisau Regency are composed of alluvium formations [10]. This location were formed during the Holocene era, along with fiery rock formations [11]. Alluvium formations are composed of clay, kaolinite, dust, sand, peat, crust, and loose chunks, which are river and swamp deposits [10], [5]. The volcanic rock formation comprises greenish-gray volcanic breccia with components consisting of andesite, basalt, and chert. These materials are associated with basalt [10]. The Peatland in Pulang Pisau Regency is experiencing several ecological problems, such as drought and land fires during the dry season and flooding during the rainy season [12]. Therefore, Pulang Pisau Regency's peatland dynamics require regular monitoring using remote sensing satellite technology. This technology was chosen because it can be applied to a large area at a lower cost [13], [14]. The dynamics of Peatland are in the form of land subsidence [15]. Land subsidence in Peatland has been monitored using the latest Digital Terrain Model (DTM) every 6 to 7 months, starting in January 2018. The latest DTM is extracted from the integration of the DTM master with displacement. First, DTM master results from Interferometric Synthetic Aperture Radar (InSAR) extraction of ALOS PALSAR-2 images, and then it converted from Digital Surface Model (DSM) to DTM. DTM master began using data with the acquisition in December 2017. The displacement parameter is obtained from the Differential SAR (DInSAR) of Sentinel-1 imagery [16], [17]. The advantage of this latest DTM is that it can be updated consistently using the Sentinel-1 image. Monitoring land subsidence in Peatland usually only focuses on vertical displacement [18], [19], [20]. We use the latest DTM because it can visualize the current topographical conditions. Therefore, the latest DTM can be used to solve DTM problems in Indonesia. Currently,
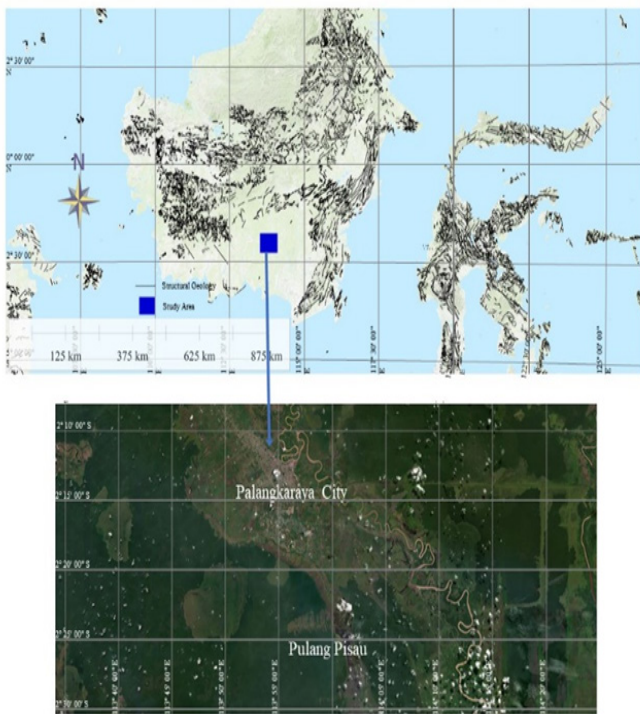
Figure 1: Study area on dynamics peatland monitoring using the latest DTM. The study areas for this research are located in the northern part of Pulang Pisau Regency, Central Kalimantan, Indonesia. Peatland and oil palm plantations dominate this area. This area has deep peat domes and represents the overall peatland conditions in Pulang Pisau Regency

the available DEM in Indonesia is DEMNAS. It was produced in 2010. DEMNAS is the fusion of DSM IFSAR, DSM TerraSAR-X, and DSM ALOS PALSAR. The condition of DEMNAS is no longer able to describe the current topographical conditions, especially in fault areas with high deformation, active volcanoes, and peatlands which are very dynamic in their land dynamics. These dynamic conditions can be monitored with the latest DTM. The Pulang Pisau peatland is a dynamic area, and the national DSM has not monitored changes in dynamics. The national DSM in Pulang Pisau has not visualized the latest terrain conditions [21]. The latest DTM can visualize the terrain conditions and the dynamics of land changes at any time needed. This research's novelty lies in the ability to monitor the dynamics of Peatland in Pulang Pisau with the latest DTM every rainy and dry season. This study aims to monitor peatland dynamics using the latest DTM in Pulang Pisau every rainy and dry season. The latest DTM is expected to monitor vertical changes (land subsidence) with precision and better vertical accuracy.

MATERIALS AND METHODS

During this research, peatland dynamics detection used a remote sensing approach to monitor the dynamic topography in Peatland using the latest DTM every 6 to 7 months. Then, a comparative analysis of changes in dynamics was carried out with profiling on peatlands.

The latest DTM was built using the ALOS PALSAR-2 and Sentinel-1 integration. ALOS PALSAR-2 is used to generate a DTM master. The vertical displacement is extracted using Sentinel-1. The DTM Master and the displacement used a similar height reference field. The height reference field of DTM Master and the displacement both used EGM 2008. The latest DTM was obtained from the integration of the DTM master with the displacement. The latest DTM is extracted by using three combination methods. The methods are InSAR, DSM to DSM master conversion, and displacement using DInSAR. DTM master is the result produced by InSAR ALOS PALSAR-2. The steps taken included data preparation, interferogram generation and adaptive filters, phase unwrapping, refinement, re-flattening, DSM extraction with phase to height, height error correction, and converting DSM to DTM [22], [23]. The ALOS PALSAR-2 data used was the raw level data (1.0). There were at least two data sets used. Both data sets functioned as master data and slave data [24]. This data preparation included focusing and Single Looks Complex (SLC) [25]. The SLC file is the primary data used for the InSAR stages [26]. The next step was interferogram generation and adaptive filtering. This stage aimed to determine the coherence value of master data and slave data used [27]. Goldstein filter was selected to display smoother processing results [28], [29]. The third stage was the phase of unwrapping. This stage aimed to reduce the noise that occurred in the interferogram and facilitate the image's interpretation. The method used in this phase unwrapping was minimum cost flow (MCF) [16]. The fourth stage was refinement and re-flattening. Around 100 tie points were made on both images simultaneously, with a minimum error of 3σ [30]. The fifth stage was DSM extraction with phase to height. However, the resulting DSM still included height errors, and it was necessary to carry out height error correction [31]. This correction aimed to eliminate anomalies in the DSM and the eight neighboring pixels with a tolerance of 2σ [32]. The next stage was DSM to DTM master conversion. The parameter used at this stage was a radius of 20 m with a slope angle of 200. The final result on the ALOS PALSAR-2 data was the DTM master. This DTM master was used as the reference DTM for the latest DTM extraction. Displacement extraction used DInSAR of Sentinel-1 data. Displacement was extracted every 6 to 7 months. In this study, the displacement periods were January 2018, August 2018, January 2019, July 2019, January 2020, and June 2020. Displacement extraction during one of these periods used a minimum of two Sentinel-1 images [27], [33], [34]. Both Sentinel-1 images used SLC level data [34]. The stages taken were DInSAR. These stages of this method were mostly similar to those of InSAR but included one different stage. It involved replacing the creation of DSM displacement with "phase to displacement" [17], [19], [27], [35], [36]. The displacement results during this process also need to be corrected for height errors [37], [38]. The next stage was the latest DTM extraction with the integration of the

DTM master and displacement. The latest DTM produced was in January 2018, August 2018, January 2019, July 2019, January 2020, and June 2020. This condition is a dynamic condition that occurs in Peatland. The six combinations of the latest DTM will describe the condition of surface change in peatlands. Six of the latest DTM with a different period (rain and dry season). Dynamic topographic conditions can be determined by making a cross-section profile. The cross-section is made to visualize the profile of rivers and swamps in the lowland. This condition will visualize the dynamic topographic conditions based on six periods of the latest DTM. The subsidence and uplift conditions in rivers and swamps on peatlands are monitored based on the cross-section profile. The latest DTM that has been produced will require a vertical accuracy evaluation. The latest DTM was obtained from the combined DTM master and the latest vertical displacement. Vertical shifts occur in tectonic areas with dip-slip faults, while horizontal shifts occur in tectonic areas with strike-slip faults. Therefore, the latest DTM represents the latest topographic conditions.

RESULTS

The DTM Master obtained is the result of interferometric processing from ALOS PALSAR-2; see Figure 2. This area has an elevation between -3 and 50 m. Land subsidence generally occurs in areas with an elevation of <25 m. The spatial resolution of this DTM master is 5 m, with a vertical accuracy of 2–3 m. River basins and swamp areas have relatively flat landforms with elevation values of around -3 to 5 m.
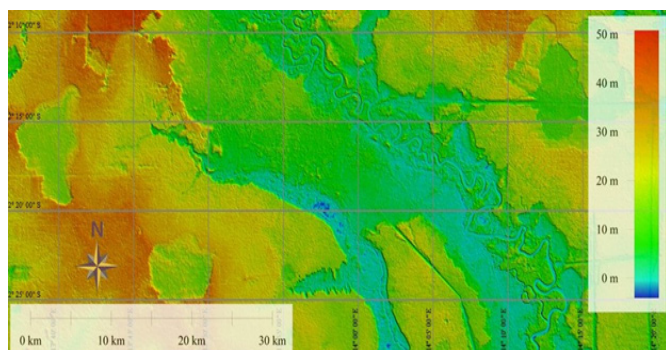

Figure 2: DTM master was extracted from InSAR ALOS PALSAR-2. This DTM master was a DTM topographic condition from December 2017

Displacement was extracted from the Sentinel-1 image. The latest DTM was extracted from the integration of the DTM master and the latest displacement. The extraction results were generated in January 2018, August 2018, January 2019, July 2019, January 2020, and June 2020; see Figure 3 and Figure 4. In June 2020, the displacement extraction values were in the range of -0.240 to 0.196 cm. This value is the displacement in June 2020 for the DTM master. Lowland areas such as Peatland and oil palm plantations experience high land subsidence. One of the reasons for the lack of surface water

is the weakness of those methods. Therefore, there is significant subsidence; meanwhile, in June 2020, there was a dry season. In August 2018, there was an increase in Peatland. One of the causes for this was the supply of surface water in the study area to peatland and oil palm plantations. In January 2019, there was an increase in the surface of Peatland. This condition was due to an increase in surface water flow as the product of rainwater supply. During this month, there was high rainfall in the studied area. As a result, the displacement value that occurred was around -0.360 to 0.520 m. Therefore, the dominance of displacement in this period is positive. In July 2019, the displacement that occurred was -0.120 to 0.428 m. In general, during this period, the displacement that occurred was -0.120 to 0.2 m. In January 2020, the land subsidence that occurred was -0.72 to 1.20 m. During this period, land subsidence was dominated by a decline of -0.25 m. Areas that experience land subsidence is located around swamps, rivers, and oil palm plantations.

DISCUSSION

Based on the results obtained, it can be seen that the location of this study is predominantly experiencing land subsidence. The latest DTM with DEMNAS (oldest DTM) can be visualized the difference in vertical accuracy and the difference in topographic elevation values at the same point. In Figure 3, we can see a comparison between the latest DTM with DEMNAS (old DTM).
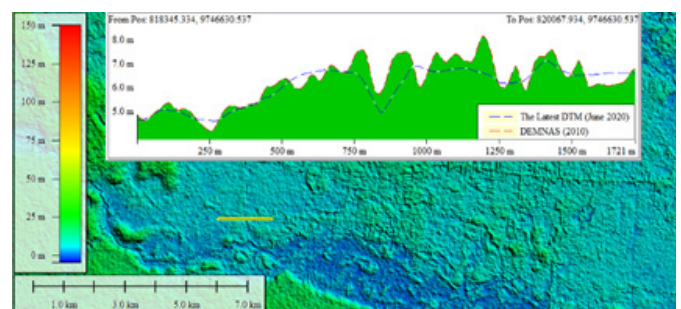

Figure 3: The difference between the Latest DTM (June 2020) with DEMNAS (old DTM 2010)

The red color is the topographical height value in 2010, while the blue color was the topographical height value in June 2020. The difference between the two topographical heights is about 0.5 to 1.5 m. This difference indicates the occurrence of subsidence from 2010 to 2020. In some areas, there has been an uplift, but it is not of great value. In general, the peatland area is experiencing subsidence. This condition indicates that DEMNAS (old DTM) cannot be used for mapping applications in areas with high dynamics, such as peatlands and areas of high vertical deformation. The latest DTM can be used as a solution to the problem of DTM scarcity in Indonesia.

Comparison of Land Subsidence from the Latest DTM 2018-2020

Land subsidence extraction from the latest DTM can be monitored by checking the cross-section profile in the study area. A random cross-section profile check is carried out every period to determine the area's land subsidence condition. This check is carried out in a similar area in each period. From January 2018 to June 2020, the topographic dynamics had dynamic values. The peatlands have significant experience in land subsidence. From January 2018 to August 2018, the topographic dynamics had a value of 1.45 to 1.60 m. Topographical dynamics in the January 2019 period experienced a decline in value. The topographic dynamics in August 2018 to January 2019 period amounted to 0.13 to 0.21 m. The value of topographical dynamics again increased in the latest DTM in July 2019. The dynamic value in January 2019 to July 2019 period was 0.40 to 0.55 m. During July 2019 to January 2020 period, there was a decline in the value of topographic dynamics on peatlands. The value in this period was 0.07 to 0 m. Finally, the period of January 2020 to June 2020 also experienced changes in topographic dynamics. In this period, there was an increase of 0.25 to 0.35 m. The rainy season and dry season conditions significantly affect groundwater conditions at the surface and groundwater in peatlands. Figure 4 is the comparison of the land subsidence on Peatland from January 2018 to June 2020. Changes in the water level in peatlands can cause land subsidence and uplift in peatlands. Peatlands will experience high topographic dynamics compared to areas that experience deformation in tectonic, volcanic, and tectonic landscapes. A complete view regarding land subsidence in each period. In this area, land subsidence changes occurred at a value of -0.259 m to 0.165 m from January 2018 to June 2020. The most change was at -0.016 to 0.014 m. The next most extensive changes were -0.047 to 0.016 and -0.077 m to -0.047 m. Suppose the change in land subsidence is made into an area experiencing upward and downward vertical deformation. The difference in the months chosen during the dry season is due to Sentinel-1 data's availability and the maximum temperature conditions in the dry season. The dynamics of peatlands are in the form of land subsidence. The highest land subsidence occurred in January 2020, while the lowest land subsidence occurred in August 2020. The area with elevation (5 to 15 m) has increased land subsidence or vertical uplift deformation. The value lies in the range of 0 to 0.196 m. Conversely, the area with elevation (-3 to 5 m) has decreased land subsidence. This value lies in the range of 0 to 0.240 m. In general, the study area experienced a decrease in land subsidence. Pulang Pisau Regency also experienced a decline, as did oil palm plantations, swamps, and peatlands. Areas that have experienced an increase in land subsidence are located near rivers and dense forests on peatlands. In the river area, there is sedimentation due to the dry season. From January 2018 to January 2020, information on land sub-

sidence distribution on the peatlands was also collected. In this period, there was a decrease in vertical deformation of 0 to -0.72 m. The decline occurred in Pulang Pisau Regency, plantation land, and peatlands. The area that experienced an increase was the northeastern part of the Pulang Pisau Regency. One possibility for this area to experience an increase could be the area clearing oil palm land. When clearing oil palm land, flow is often carried out in the opening canals. This condition requires enormous amounts of water so that peatlands in plantation lands experience an increase in elevation due to water seeping into the peatlands.

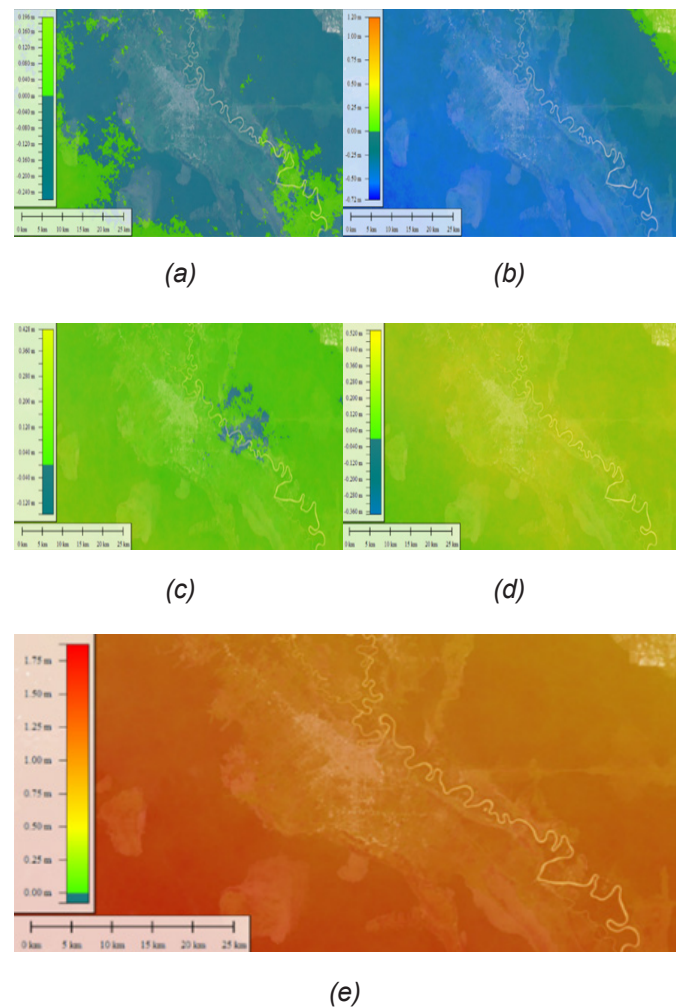*(a)*   *(b)*

(c)   *(d)*

(e)

Figure 4: Comparison of the land subsidence on Peatland from January 2018 to June 2020. The latest DTM is extracted every 6 to 7 months, namely January 2018, August 2018, January 2019, July 2019, January 2020, and June 2020. (a) the land subsidence from January 2020 to June 2020. (b) the land subsidence from July 2019 to January 2020. (c) the land subsidence from January 2019 to July 2019. (d) the land subsidence from August 2018 to January 2019. (e) the land subsidence from January 2018 to August 2018.

In the period from January 2018 to July 2019, this region experienced an increase in land subsidence. In general, the increase in land subsidence lies in the value range of 0 to 0.428 m. The area that is experiencing decline is located in the swampy part of the eastern city of Pulang Pisau. The range of values for the decline is from 0 to -0.12 m. From January 2018 to January 2019, in general, this region experienced an increase in land subsidence. However, only a small proportion of them experienced a decrease in land subsidence. The increase in land subsidence lies in the range of 0 to 0.52 m. It increased due to an increase in surface water flow during the period from February to January 2019. This increase can be seen in the information on land subsidence in the early January to August 2018 period. It is located in the range of 0 to 1.75 m. Although the land subsidence comparison can be made based on the latest DTM, comparisons can be made according to the period. Figure 4 compares land subsidence based on the latest DTM on Peatland from January 2018 to June 2020.

Vertical Accuracy Test of the Latest DTM in Peatland

Checking the vertical accuracy test on the latest DTM was carried out in two ways. The methods used were checking the river profile and checking the swamp in the lowland profile. This profile check was meant to determine the dynamics profile changes at each of the latest DTM periods. Profile checking was carried out on the shape of the river. The latest DTM displays the curvature of the river so that it resembles the real conditions. The shape of the river's curvature is checked on each river, water channel, and stream. Overall, the latest DTM can display rivers, waterways, and swamps in lowlands; see Figure 5. However, the latest DTM is biased for surface runoff and contouring in areas around rivers and lowlands. Checking this curvature still requires checking with Global Navigation Satellite System (GNSS)-leveling. This step was used to check the cross-section profile of the swamps in the lowlands area. It is located at an elevation of -3 to 5 m. These lowland areas are generally swamps located adjacent to rivers. This area is checked by making an extended profile. The elevation value was extracted at each latest DTM from January 2018, August 2018, January 2019, July 2019, January 2020, and June 2020. All the latest DTM were compared to their elevation values. It was done in order to obtain a dynamics visualization of the peatlands. The elevation in August 2018 had a higher elevation than other DTMs. The latest DTM in January had the lowest elevation. The rainy season and dry season affected the dynamics of these peatlands. Land subsidence is influenced by the amount of water contained in the peatlands. Weather anomalies that occur in Kalimantan also affect the dynamics of Peatland. As in August 2018, there should have been a dry season, but there was heavy rain around the image acquisition date, so that the land dynamics would be high elevation. Under average weather conditions, June, July,
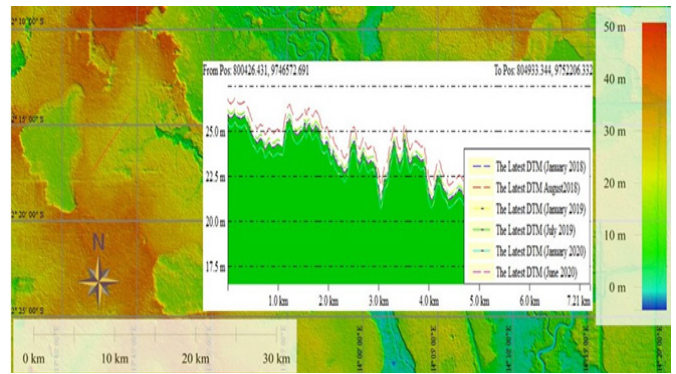

Figure 5: Comparison of land subsidence based on the latest DTM on Peatland from January 2018 to June 2020. The latest DTM is extracted every 6 to 7 months, namely January 2018, August 2018, January 2019, July 2019, January 2020, and June 2020.

and August will experience land subsidence. As in the latest DTM in July 2019, this land experienced a dry season, and land fires occurred. As a result, almost all elevations on Peatland experienced land subsidence of 10 to 80 cm. Another land subsidence anomaly also occurred in January 2020. Since it rarely rains from December to January 2020, this causes drought on the peatlands. The drought caused land subsidence of 10 to 100 m. Checks for lowland areas were also carried out elsewhere. The location is far from the river. This region has an elevation of -0.5 to 4 m. The rainy season and dry season affect the land subsidence condition in the peatlands. Weather anomaly factors also affect the wetness of peatlands. The highest land subsidence in this area occurred in January 2019. Another check was carried out in peatland areas, which already had a slight variation in topography between -0.5 and 5 m. The cross-section profile created was located between 2 low hills and had a low elevation of less than 20 m. In this region, land subsidence conditions are more diverse. At an elevation of -0.5 to 3 m, there are visible land dynamics and higher land subsidence conditions. In another case, at an elevation of 4 to 5 m, the land subsidence decreased. Changes in land subsidence every 6 to 7 months in the latest DTM are low value, and peatland dynamics are starting below. A vertical accuracy test is done by comparing the latest DTM with field data (GNSS-levelling). Based on Table 1, The latest DTM has a Root Mean Square Error (RMSE (z)) of 0.705 m on the field measurement. All height differences between the latest DTM and the field measurement were less than 1 m. This condition is because the study area has a relatively flat topography and a low slope (< 10%). Therefore, the results of this vertical accuracy test only apply to areas with relatively flat topography. This vertical accuracy test uses 15 measurement points from GNSS leveling. Based on the RMSE (z) obtained, the latest DTM vertical accuracy is 1.3818 m at the 95% confidence level. The vertical accuracy value corresponds to a mapping scale of 1: 10,000 to 1: 20,000. In these conditions, the latest DTM can be an alternative DEM

Table 1: Comparison of the latest DTM with field measurement

X (m)	Y (m)	The atest DTM (m)	Field measurement (m)	ΔH (Latest vs. field) (m)
828,051.6	9,746,366.7	8.115	8.8	0.685
828,320.6	9,746,274.3	7.407	8.8	1.393
828,008.6	9,746,183.2	8.291	9.8	1.509
827,793.1	9,745,840.4	7.643	7.3	0.343
827,634.7	9,745,582.3	7.629	7.2	0.429
827,441.5	9,745,691.8	7.590	8.1	0.510
826,969.8	9,746,036.0	6.482	5.8	0.682
826,671.8	9,745,896.9	3.608	4.5	0.892
826,795.5	9,746,172.4	6.668	5.7	0.968
826,490.8	9,746,375.9	7.608	6.9	0.708
826,531.2	9,745,519.0	5.185	6.1	0.915
825,807.1	9,745,779.9	5.799	6.2	0.401
827,427.7	9,745,134.7	5.694	5.7	0.006
827,033.2	9,745,634.4	7.500	6.7	0.800
826,098.0	9,746,186.6	6.141	5.8	0.341
Sum				10.58
RMSE (z)				0.705

for mapping in lowlands and peatlands. The latest DTM has been used for various basic mapping and thematic mapping applications in Indonesia.

CONCLUSION

This research concludes that monitoring peatland dynamics would benefit from the use of the latest DTM. In the study area in Pulang Pisau Regency, peatland monitoring used six periods with the latest DTM. The periods monitored were January 2018, August 2018, January 2019, July 2019, January 2020, and June 2020. The dynamics of peatlands varied from -1.5 to 1.5 m. It was due to the stability of the soil and the water levels in the peatlands. The elevation in the latest DTM varies with land subsidence and uplift. Different conditions in each period were also influenced by the rainy and dry seasons. The latest DTM is extracted from the integration of InSAR ALOS PALSAR-2 with DInSAR Sentinel-1. The latest DTM has an RMSE(z) of 0.705 m on the field measurement. This vertical accuracy test uses 15 measurement points from GNSS-leveling. Based on the RMSE (z) obtained, the latest DTM vertical accuracy is 1.3818 at the 95% confidence level. The latest DTM has a spatial resolution of 5 m and can be used at a mapping scale of 1: 10,000–1: 20,000.

AUTHOR STATEMENT

We would like to submit this manuscript named "Dynamic topography monitoring in peatland using the latest Digital Terrain Model" for possible evaluation for publishing. We certify that the paper is the original work and has not been published before.

REFERENCES

1. Kentucky Geological Survey (KGS), "Coal Information," Kentucky Geological Survey, University of Kentucky. https://www.uky.edu/KGS/coal/coal-use.php. (2016).

2. Houghton, R. A. et al., "Carbon emissions from land use and land-cover change," vol. 4, pp. 5125–5142, DOI: 10.5194/bg-9-5125-2012. (2012).

3. Konecny, K. et al., "Variable carbon losses from recurrent fires in drained tropical peatlands," Glob. Chang. Biol., vol. 22, no. 4, pp. 1469–1480, DOI: 10.1111/gcb.13186. (2016).

4. Reddington, C. L., Balasubramanian, R., Spracklen, D., "Contribution of vegetation and peat fires to particulate air pollution in Southeast Asia," no. February 2015, 2014, DOI: 10.1088/1748-9326/9/9/094006. (2015).

5. Cahyono, B. K., Aditya, T., Istarno, "The least square adjustment for estimating the tropical peat depth using LiDAR data," Remote Sens., vol. 12, no. 5, DOI: 10.3390/rs12050875. (2020).

6. Winantris, W., Hamdani, H., Harlia, E. "Paleoenvironment of Tanjung Formation Barito Basin- Central Kalimantan Based on palynological data," J. Geosci. Eng. Environ. Technol., vol. 2, no. 2, p. 110, 2017, DOI: 10.24273/jgeet.2017.2.2.305. (2017).

7. Asmuß, T., Bechtold, M., Tiemeyer, B. "On the Potential of Sentinel-1 for High Resolution Monitoring of Water Table Dynamics in Grasslands on Organic Soils," Remote Sens., vol. 11, no. 14, p. 1659, DOI: 10.3390/rs11141659. (2019).

8. Julzarika, A., Setiawan, K. T. "Utilization of SAR and Earth Gravity Data for Sub Bituminous Coal Detection," Int. J. Remote Sens. Earth Sci., vol. 11, no. 2, p. 143, Apr., doi: 10.30536/j.ijreses.2014.v11.a2612. (2017).

9. Badan Pusat Statistik, Statistik Daerah Kabupaten Pulang Pisau Tahun 2020. (2020).

10. Abidin, H. Z., "The tectonic history and mineral depostit of easte-west Kalimantan .pdf," University of Adelaide, (1998).

11. Purnama, A., Huda, M. "A preliminary study of Indonesian coal basins for underground coal gasification development," Indones. Min. J., vol. 22, no. 1, pp. 61–76, DOI: 10.30556/imj.vol22.no1.2019.275. (2019).

12. McPartland, M. et al., "Characterizing Boreal Peatland Plant Composition and Species Diversity with Hyperspectral Remote Sensing," Remote Sens., vol. 11, no. 14, p. 1685, DOI: 10.3390/rs11141685. (2019).

13. Trisakti, B., Julzarika, A., Nugroho, U. C., Yudhatama, D., Lasmana, D., "Can the Peat Thickness Classes be Estimated from Land Cover Approach?," Int. J. Remote Sens. Earth Sci., vol. 14, no. 2, p. 93, Jan. 2018, DOI: 10.30536/j.ijreses.2017.v14.a2677. (2018).

14. Vernimmen, R. et al., "Mapping deep peat carbon stock from a LiDAR based DTM and field measurements, with application to eastern Sumatra," Carbon Balance Manag., vol. 15, no. 1, pp. 1–18, DOI: 10.1186/s13021-020-00139-2. (2020).

15. Siegert, F. et al., "International Peat Mapping Team (IPMT)," (2018).

16. Costantini, M., "A novel phase unwrapping method based on network programming," IEEE Trans. Geosci. Remote Sens., vol. 36, no. 3, pp. 813–821, DOI: 10.1109/36.673674. (1998).

17. Devanthéry, N., Crosetto, M., Cuevas-González, M., Monserrat, O., Barra, A., Crippa, B., "Deformation Monitoring Using Persistent Scatterer Interferometry and Sentinel-1 SAR Data," Procedia Comput. Sci., vol. 100, pp. 1121–1126, doi: 10.1016/j.procs.2016.09.263. (2016).

18. Venera, J., Anton, F., Irina, K., Alena, Y., "SAR Interferometry Technique for Ground Deformation Assessment on Karazhanbas Oilfield," Procedia Comput. Sci., vol. 100, pp. 1163–1167, DOI: 10.1016/j.procs.2016.09.271. (2016).

19. Caló, F., "DInSAR-based detection of land subsidence and correlation with groundwater depletion in konya plain, Turkey," Remote Sens., vol. 9, no. 1, DOI: 10.3390/rs9010083. (2017).

20. Lubis, A. M., Sato, T., Tomiyama, N., Isezaki, Yamanokuchi, N., "Ground subsidence in Semarang-Indonesia investigated by ALOS-PALSAR satellite SAR interferometry," J. Asian Earth Sci., vol. 40, no. 5, pp. 1079–1088, DOI: 10.1016/j.jseaes.2010.12.001. (2011).

21. Julzarika, A., Harintaka, "Indonesian DEMNAS: DSM or DTM?," in 2019 IEEE Asia-Pacific Conference on Geoscience, Electronics and Remote Sensing Technology (AGERS), pp. 31–36, DOI: 10.1109/AGERS48446.2019.9034351. (2020).

22. Hooper, A., Bekaert, D., Spaans, Ar, M., "Tectonophysics Recent advances in SAR interferometry time series analysis for measuring crustal deformation," vol. 517, pp. 1–13, DOI: 10.1016/j.tecto.2011.10.013. (2013).

23. Castellazzi, P., Garfias, J., Martel, Brouard, C., Rivera, A., "InSAR to support sustainable urbanization over compacting aquifers: The case of Toluca Valley, Mexico," Int. J. Appl. Earth Obs. Geoinf., vol. 63, (2017}, DOI: 10.1016/j.jag.2017.06.011.

24. Lusch, D. P., "Introdcution to Microwave Remote Sensing," DOI: 10.1111/j.1477-9730.2009.00531_1.x. (1999).

25. Zuo, R., Qu, C., Shan, X., Zhang, G, X. Song., "Tectonophysics Coseismic deformation fields and a fault slip model for the Mw 7.8 mainshock and Mw 7.3 aftershock of the Gorkha-Nepal 2015 earthquake derived from Sentinel-1A SAR interferometry," Tectonophysics, vol. 686, pp. 158–169, DOI: 10.1016/j.tecto.2016.07.032. (2016).

26. Lanari, R., Mora, O., Manunta, M., Mallorquí, J. J., Berardino, P., Sansosti, E., "A small-baseline approach for investigating deformations on full-resolution differential SAR interferograms," IEEE Trans. Geosci. Remote Sens., vol. 42, no. 7, pp. 1377–1386, DOI: 10.1109/TGRS.2004.828196. (2004).

27. Strozzi, T. et al., "Satellite SAR interferometry for the improved assessment of the state of activity of landslides: A case study from the Cordilleras of Peru," Remote Sens. Environ., vol. 217, no. August, pp. 111–125, DOI: 10.1016/j.rse.2018.08.014. (2018).

28. Baran, I., Stewart, M. P., Kampes, B. M., Perski, Z., Lilly, P., "A modification to the Goldstein radar interferogram filter," IEEE Trans. Geosci. Remote Sens., vol. 41, no. 9 PART II, pp. 2114–2118, doi: 10.1109/TGRS.2003.817212. (2003).

29. Sun, Q., Li, Z. W., Zhu, J. J., Ding, X. J., Hu, J., Xu B., "Improved Goldstein filter for InSAR noise reduction based on local SNR," J. Cent. South Univ., vol. 20, no. 7, pp. 1896–1903, DOI: 10.1007/s11771-013-1688-3. (2013).

30. Li, L., Kuai, X., "An efficient dichotomizing interpolation algorithm for the refinement of TIN-based terrain surface from contour maps," Comput. Geosci., vol. 72, pp. 105–121, DOI: 10.1016/j.cageo.2014.07.001. (2014).

31. Wessel, B., Huber, B., Wohlfart, C., Marschalk, U., Kosmann, D., Roth, A., "Accuracy assessment of the global TanDEM-X Digital Elevation Model with GPS data," ISPRS J. Photogramm. Remote Sens., vol. 139, DOI: 10.1016/j.isprsjprs.2018.02.017. (2018).

32. Rizzoli, P., Bräutigam, B., Kraus, T., Martone, M., Krieger, G., "Relative height error analysis of TanDEM-X elevation data," ISPRS J. Photogramm. Remote Sens., vol. 73, no. 2012, pp. 30–38, doi: 10.1016/j.isprsjprs.2012.06.004. (2012).

33. Dias, P., Catalao, J., Marques, F. O., "Sentinel-1 InSAR data applied to surface deformation in Macaronesia (Canaries and Cape Verde)," Procedia Comput. Sci., vol. 138, pp. 382–387, DOI: 10.1016/j.procs.2018.10.054. (2018).

34. Rucci, A., Ferretti, A., Monti Guarnieri, A., Rocca, F., "Sentinel 1 SAR interferometry applications: The outlook for sub-millimeter measurements," Remote Sens. Environ., vol. 120, pp. 156–163, DOI: 10.1016/j.rse.2011.09.030. (2012).

35. Julzarika, A., Harintaka, "Utilization of Sentinel Satellite for Vertical Deformation Monitoring in Semangko Fault-Indonesia," ACRS, pp. 1–7, (2019).

36. Mullissa, A. G., Tolpekin, V., Stein, A., Perissin, D., "Polarimetric differential SAR interferometry in an arid natural environment," Int. J. Appl. Earth Obs. Geoinf., vol. 59, pp. 9–18, DOI: 10.1016/j.jag.2017.02.019. (2017).

37. An, W., Carlsson, W. E., "Speckle interferometry for measurement of continuous deformations," Opt. Lasers Eng., vol. 40, no. 5–6, pp. 529–541, DOI: 10.3390/ma6051656. (2003).

38. Malinowska, A. A., Witkowski, W. T., Guzy, A., Hejmanowski, R., "Mapping ground movements caused by mining-induced earthquakes applying satellite radar interferometry," Eng. Geol., vol. 246, no. October, pp. 402–411, doi: 10.1016/j.enggeo.2018.10.013. (2018).